Evidence of phytoplankton light acclimation to periodic turbulent mixing along a tidally dominated tropical coastline.

Martin James McLaughlin[1], Jim Greenwood[2], Paul Mathew Branson[1], Martin J Lourey[3], and Christine E Hanson[4]

[1]CSIRO
[2]Commonwealth Scientific and Industrial Research Organisation (CSIRO)
[3]BMT Global
[4]Department of Education WA

November 24, 2022

Abstract

One of the largest tropical tidal ranges in the world occurs in King Sound, a semi-enclosed embayment in the tropical Kimberley region of Western Australia. Incubations of phytoplankton within King Sound displayed reduced photosynthetic efficiency, elevated maximum photosynthetic rates, and no measurable photo-inhibition. A response typical of high light adapted phytoplankton despite decreased water clarity and low ambient nutrient concentrations in the estuary. This is in contrast with the adjacent shelf where phytoplankton, associated with a deep chlorophyll maximum, display high photosynthetic efficiency, and strong light inhibition typical of low light adaptation. Remote sensing and numerical modelling suggest that spatial and temporal variations in tidal mixing drive changes in light variability and in photo-acclimation. In King Sound phytoplankton experience the largest variations in light over short timescales where diatoms dominate since they can rapidly acclimate to water column light conditions by adjusting pigment within the cell. The photo-physiological response of the phytoplankton in the Sound, suggests that acclimation to alternate weak and strong mixing exposes them to cyclical changes in light intensity delaying the onset of photo-inhibition, allowing higher maximum photosynthetic rates to be attained. These findings highlight the importance of a multifaceted approach to understanding the links between physics and photo-acclimation strategies employed by phytoplankton to more accurately determine rates of depth-integrated productivity in complex coastal areas.

Evidence of phytoplankton light acclimation to periodic turbulent mixing along a tidally dominated tropical coastline.

M.J. McLaughlin[1,2]*, J. Greenwood[1], P. Branson[1,2], M.J. Lourey[3], C.E. Hanson[4]

[1]CSIRO Oceans and Atmosphere, Indian Ocean Marine Research Centre, M097, 64 Fairway, Crawley, Western Australia 6009

[2]University of Western Australia, Oceans Institute, Indian Ocean Marine Research Centre, M470 35 Stirling Highway, Crawley, Western Australia, 6009.

[3]BMT Global, 4/20 Parkland Rd, Osborne Park, Western Australia 6017, Australia

[4]Department of Education WA, 151 Royal Street, East Perth, Western Australia, 6004

1

2

3   * Corresponding author: Tel.: +61-8-9333-6523. E-mail address: james.mclaughlin@csiro.au

4   * ORCHID ID - 0000-0002-9936-1919

5

6

7

8   **Key Points**

9   • Variations to vertical mixing & light attenuation drives partitioning of phytoplankton taxa through
10   differing photo-acclimation strategies.

11

12   • Offshore phytoplankton acclimated to dark conditions with strong photo-inhibition at a deep
13   chlorophyll maximum.

14

15   • Nearshore/estuarine phytoplankton photo-acclimated to high light with elevated photosynthetic rates
16   and no observed photo-inhibition.

17

18 **Abstract**

19 One of the largest tropical tidal ranges in the world occurs in King Sound, a semi-enclosed embayment in

20 the tropical Kimberley region of Western Australia. Incubations of phytoplankton within King Sound

21 displayed reduced photosynthetic efficiency, elevated maximum photosynthetic rates, and no measurable

22 photo-inhibition. A response typical of high light adapted phytoplankton despite decreased water clarity and

23 low ambient nutrient concentrations in the estuary. This is in contrast with the adjacent shelf where

24 phytoplankton, associated with a deep chlorophyll maximum, display high photosynthetic efficiency, and

25 strong light inhibition typical of low light adaptation. Remote sensing and numerical modelling suggest that

26 spatial and temporal variations in tidal mixing drive changes in light variability and in photo-acclimation. In

27 King Sound phytoplankton experience the largest variations in light over short timescales where diatoms

28 dominate since they can rapidly acclimate to water column light conditions by adjusting pigment within the

29 cell. The photo-physiological response of the phytoplankton in the Sound, suggests that acclimation to

30 alternate weak and strong mixing exposes them to cyclical changes in light intensity delaying the onset of

31 photo-inhibition, allowing higher maximum photosynthetic rates to be attained. These findings highlight the

32 importance of a multifaceted approach to understanding the links between physics and photo-acclimation

33 strategies employed by phytoplankton to more accurately determine rates of depth-integrated productivity

34 in complex coastal areas.

35

36

2

37   **Plain Language Summary**

38   The Southern Kimberley Coast in Australia's Northwest is dominated by the largest tides in the world's

39   tropical regions, and second only to the Bay of Fundy in Canada. King Sound the main feature of this

40   region, is a 100-km-long, semi-enclosed embayment opening to the Indian Ocean. Tidal mixing is an

41   important control on phytoplankton distribution in shallow coastal macrotidal regions like this. Despite low

42   ambient nutrients and decreased water clarity in King Sound, phytoplankton showed a photo-acclimation

43   strategy suited to high light exposure. This is in contrast with the adjacent shelf where phytoplankton,

44   associated with a deep chlorophyll maximum, displayed a photo-acclimation strategy more suited to low

45   light.   King Sound experiences the largest variations in light over short timescales and we found the

46   phytoplankton were dominated by diatoms since they can rapidly adjust pigment within the cell to acclimate

47   to water column light conditions. Observations from remote sensing and numerical modelling suggest that

48   spatial and temporal variations in tidal mixing drive changes in light variability and in photo-acclimation. The

49   acclimation by phytoplankton to alternate weak and strong mixing exposes them to cyclical changes in light

50   intensity delaying the onset of photo-inhibition, allowing higher maximum photosynthetic rates to be

51   attained.

1 Introduction

Tidal mixing is an important control on phytoplankton distribution in estuaries (Cloern, 1991; Lucas *et al.*, 1999; Trigueros & Orive, 2000) and in shallow coastal macrotidal regions of the coastal sea (Blauw *et al.*, 2012, Houliez *et al.*, 2013). Tides induce horizontal and vertical mixing, which redistributes phytoplankton and nutrients, influencing community structure and phytoplankton population dynamics (Lewitus *et al.*, 1998; Domingues *et al.*, 2010). Despite several observations of tidally driven variability in estuarine phytoplankton biomass and taxonomic composition (Jouenne *et al.*, 2005; Wetz *et al.*, 2006; Domingues *et al.*, 2010; Blauw *et al.*, 2012), the impact of tides on phytoplankton productivity has not been well investigated. Measurements of phytoplankton photosynthetic rates are critical to provide accurate predictions of primary production and biogeochemical processes, important components of carbon cycling, under the variable conditions that commonly define estuarine and coastal marine environments. Here, we are primarily concerned with the effect that vertical tidal mixing has on phytoplankton photo-physiology, and its implicit effect on the overall rate of carbon fixation.

The importance of photo-acclimation in aquatic phototrophs stems from the extreme spatial and temporal variability of the underwater light field (Dubinsky & Stambler, 2009). Photo-acclimation in a phytoplankton cell is characterized by changes in the amount and ratios of light harvesting and photoprotective pigments, in photosynthetic parameters, photosynthetic and respiratory enzymatic activities, chemical composition and cell volume (Falkowski & LaRoche, 1991). Chloroplast size and morphology (shape and structure), numbers, and distribution within the cell, can be hugely different in the various phytoplankton classes and pigment-groups (Kirk & Tilney-Bassett, 1978; Larkum & Vesk, 2003). The species-specific differences in chloroplast size and morphology in a given species is also affected by light climate (irradiance, the spectral composition of irradiance and day length). In the aquatic environment these are amplified by the superimposed steep attenuation of light by water and the substances and particles dissolved and suspended in it (Smith & Mobley, 2008). Vertical turbulent mixing of the water column can modify this situation by redistributing particles, such as phytoplankton cells or suspended sediment, and altering the upward flux of nutrients relative to the vertical light gradient. This enables cells to either escape prolonged periods near the surface where photo-inhibition can occur or prevent them from sinking below the photic

4

80 zone (Demers *et al.*, 1986). Finely coordinated mechanisms of photo-acclimation allow aquatic

81 phytoplankters to survive over a 2 order of magnitude range of ambient irradiance. Photo-acclimation to low

82 light requires adequate nutrient supply (Herzig & Falkowski, 1989, Berges *et al.*, 1996, Cardol *et al.*, 2008)

83 whereas cells that successfully acclimate to high light have difficulties in maintaining Redfield ratios through

84 sufficient nutrient uptake to keep up with the fast influx of carbon (Berman-Frank & Dubinsky, 1999).

85 Therefore, the optimal depth for phytoplankton growth is generally determined by the interrelationship

86 between opposing vertical gradients in light intensity and nutrient concentration.

87

88 The intensity and timing of tidally induced vertical mixing can influence phytoplankton photo-physiology and

89 overall productivity, as a result of changes in cell light history (Falkowski, 1980), and nutrient availability.

90 Phytoplankton, in particular diatoms, can compensate for lower light conditions by rapidly synthesising

91 more chlorophyll-*a* (chl-*a*) pigment within the cell (Sathyendranath *et al.*, 2004). When vertical mixing is

92 moderate, the environmental conditions change at a rate slower than the physiological adaptation time of

93 the phytoplankton, and the cells can continuously adapt their metabolism to these new conditions (Vincent,

94 1980). This can, for example, lead to vertical structure in phytoplankton within otherwise density uniform

95 ocean layers (Calbet *et al.*, 2015). However, when vertical mixing is persistent and sufficiently intense, and

96 environmental conditions change faster than the physiological adjustment time of phytoplankton, the cells

97 tend to adjust toward average environmental conditions (Savidge, 1979; Falkowski, 1980). The

98 physiological strategies that phytoplankton adopt in different mixing scenarios are important for maximizing

99 the efficiency of utilization of available light and photosynthetic activity (Auclair *et al.*, 1982).

100

101 The Kimberley region in the tropical North-west of Australia is a remote and biologically diverse oceanic

102 habitat. Semidiurnal, barotropic tides (Holloway *et al.*, 2001) interact with the wide (~300 km) shelf to

103 produce the second largest tidal range (up to 11 m) in the world (after Canada's Bay of Fundy; Wolanski &

104 Spagnol, 2003). The large tidal range generates strong currents (0.5 - 2 m s^{-1}; Anon, 1972). One of the

105 largest topographical features of the southern Kimberley coast is King Sound (Fig. 1), a 100-km-long, semi-

106 enclosed embayment. The Sound is characterised by extensive areas of shallow water with a mean depth

107 of 18 m, but near the mouth there is a 50 m-deep 20-km-wide channel.

108

McLaughlin *et al.* (2019) found in April/May 2010, that the waters near the mouth of King Sound, were a

phytoplankton productivity "hot-spot" despite low ambient nutrient concentration and reduced water clarity

compared with the adjacent shelf. Here, we investigate the reason for the enhanced phytoplankton

productivity within King Sound by comparing the photo-physiology of phytoplankton cells collected in the

Sound, with those collected in shelf waters. We present photo-physiological data collected at different

phases of the spring-neap (MSf) tidal cycle, and at different vertical water-column positions, across the

continental shelf including locations within King Sound. We also use satellite data and results from a

numerical model to help characterise the tidal mixing conditions in the region, and phytoplankton pigment

data to identify the dominant phytoplankton species.

118

2 Materials and Methods

2.1 Oceanographic sampling

Three cross-shelf transects were occupied during an oceanographic cruise (subsequently referred to as

SS2010) off the south-eastern section of the Kimberley coast in proximity to King Sound (KS) (13.5 - 17°S,

120 - 124°E; Fig. 1) in austral autumn (14 April - 5 May 2010). A central transect that extended into KS

was sampled twice; once on the rising spring tide, and again on the falling neap tide approximately two

weeks later. A northern and a southern transect provided greater spatial coverage of the shelf, with the

northern transect (Fig. 1; stations 27, 45 and 46) sampled 1.5 days following the spring-tide maximum, and

the southern transect (Fig. 1; stations 121, 109 and 101) sampled between 3 and 5 days following the neap

tide.

129

To evaluate cross-shelf differences in phytoplankton photo-physiology, locations near the 50 m (inner

shelf), 200 m (mid-shelf), and 1000 m (outer-shelf) isobaths were sampled on each transect. On the central

transect excursions into KS were made where a further two stations were sampled on the spring tide (Fig 1.

stations 24 and 25) and two stations during the neap (Fig 1. stations 84 and 85). Water samples were

collected using a 24 x 10 L Niskin bottle rosette with profiles of conductivity and temperature (Seabird SBE

6

135 9/11 dual-sensor unit), photosynthetically active radiation (PAR 400–700 nm; Biospherical Instruments

136 QCP-2300), and fluorescence (Chelsea Instruments Aquatracka™ fluorometer) calibrated with extracted

137 chlorophyll samples collected from the water column. Water samples from the production cast at each

138 station were collected from between 3 and 5 nominal depths (surface [~ 2 m], 10 m, 25 m, 50 m, 75 m)

139 dependent upon the bottom depth, and analysed for primary production (PP) in addition to chl-*a* and

140 phytoplankton community structure via high performance liquid chromatography (HPLC).

141

142 Vertical PAR profiles for each production cast were obtained from the on-site CTD cast closest to the sun's

143 zenith. Light profiles collected at some other nearby shelf locations occupied during the same cruise

144 (Cherukuru *et al.*, 2019) were added to provide additional information about the underwater light climate on

145 the continental shelf. Linear regression of the natural logarithm of PAR versus water-depth confirmed

146 exponential light decay in most cases providing a value of the attenuation rate k_d. For the PAR profiles

147 collected in King Sound the surface irradiance measured on the deck of the ship was used to provide an

148 additional in-water value at a nominal depth of 1 m after adjusting for sun angle and 7.6% rapid attenuation

149 following the approach of Morel (1991). Euphotic depth (z_{eu}) was calculated as the water depth where

150 irradiance is reduced to 1% of the surface value as $z_{eu} = \ln(0.01) / k_d$. We note that this is a somewhat

151 conservative estimate of the ocean's true euphotic zone (Marra et al. 2014), but it nevertheless provides a

152 useful reference for this study. For stations 24, 25, 84 and 85 occupied within King Sound the median and

153 mean PAR were also calculated according to the formulations given by Berenhfeld (2015) (median) and

154 Blain *et al.* (2013) (mean) and using a daily mean near-surface irradiance of 500 µE m^{-2} s^{-1} based on mean

155 daily records of incident PAR collected during the cruise and adjusted for sun angle and 7.6% rapid

156 attenuation at the water surface. Mixed-layer depth (l) was calculated as the depth where the value of the

157 potential density unit (σ_θ), is offset by + 0.03 kg m^{-3} compared with the value at 10 m (de Boyer-Montegut *et*

158 *al.*, 2004). For locations within King Sound where σ_θ remained above this threshold throughout the water-

159 column, the mixed-layer was assumed to extend to the seabed. The implied lack of any vertical density

160 stratification in these cases was confirmed by visual examination of the vertical profile of σ_θ.

161

162 *2.2 Satellite remote sensing and hydrodynamic model analysis*

163 Satellite remote sensing data were obtained from the Integrated Marine Observing System (IMOS) and

164 analysed in conjunction with output from a three-dimensional numerical hydrodynamic model developed for

165 the Western Australian Marine Science Institute (WAMSI). To identify the extent of persistent vertical tidal

166 mixing on the continental shelf, the spatial gradient in night-time climatological Sea Surface Temperature

167 (SST) was also calculated from the Sea Surface Temperature Atlas of the Australian Regional Seas

168 (SSTAARS) published in Wijffels *et al.* (2018).

169

170 In northern Australia, vertical mixing by the strong tidal currents act as a sink for heat and freshwater input

171 at the ocean surface. Assuming that in a given region the mixing efficiency and bed friction coefficients are

172 constant the location of the front should be defined by a critical value of h/u^3, where h is the water depth

173 and u is the surface tidal velocity amplitude (Simpson & Hunter, 1974). We utilized the results from a three-

174 month simulation with the Regional Ocean Modelling System (ROMS) to calculate the surface tidal velocity

175 amplitude as $u = u_{M2} + u_{S2}$ where u_{M2} and u_{S2} are the amplitude of the semi-major tidal ellipses for the M_2

176 and S_2 tidal constituents from a harmonic fit of the modelled surface current. The ROMS model utilized 30

177 uniformly spaced vertical sigma layers and included forcing from surface heat fluxes, freshwater input from

178 coastal catchments and applied the k-ϵ turbulence closure scheme with a quadratic bed friction coefficient

179 of 3 x 10^{-3}. For further details of the model configuration and validation see Feng *et al.* (2017).

180

181 Lewis *et al.* (1984) present a simple model that compares the relative magnitudes of the timescales of

182 photoadaptation to the timescales of irradiance fluctuations due to vertical mixing. To assess the influence

183 of vertical tidal mixing on the observations of plankton photo-physiology we estimated a mixing timescale

184 from the ROMS simulation as $T_M = l^2/K_z$ where K_z is the modelled vertical turbulent diffusivity (with units

185 m^2/s) and l is the thickness of the mixed layer. On continental shelves with large tides, increases in vertical

186 mixing during the spring tide are accompanied by increases in suspended sediment due to the increased

187 bed shear stress. At in-situ sample locations estimates of the light attenuation coefficient (k_d at 490 nm)

188 were obtained from the MODIS ocean colour satellite record from 2002 – 2020 available from IMOS (2020).

189 At each station a harmonic fit of the water surface elevation from the ROMS model was calculated to

190 provide a 20-year timeseries of predicted tide for each station. Observations of cloud-free pixels within 2 km

8

191 of each station were classified according to the tidal phase of the semi-diurnal (high water, ebb tide, low

192 water and flood tide) and spring-neap (spring, falling, neap and rising) cycles at the time of pixel acquisition

193 (see Fig. S1). Within each tide phase class, the mean and standard deviation of k_d was calculated to

194 provide an estimate of changes in irradiance length scale (k_d^{-1}) compared to the mixing length scale (l).

195

196 *2.3 Phytoplankton pigment analyses*

197 One litre of seawater from each depth was vacuum-filtered onto a Whatman 25 mm diameter glass fibre

198 filter (GF/F) (nominal pore size of 0.7 μm) and analysed for chl-*a* and phaeopigment (represents the total

199 chl-*a* fraction). The filters were stored at -20°C until analysis (24 - 48 hours post-collection), when pigments

200 were extracted in 90% acetone overnight and analysed using a calibrated Turner Designs model 10AU

201 fluorometer and the acidification technique of Parsons *et al.* (1989).

202

203 Between 1-5 L of the surface water sample were filtered onto a 25 mm, 0.7 μm, Whatman GF/F and stored

204 in liquid nitrogen until analysis. Phytoplankton pigments were extracted and analysed by High Performance

205 Liquid Chromatography (HPLC) with a Waters-Alliance system following the CSIRO protocol detailed in

206 Hooker *et al.*, (2009). In this study (as per Clementson *et al.*, 2004) pigments that relate specifically to an

207 algal class are termed marker or diagnostic pigments (Jeffrey & Vesk, 1997). Some of these diagnostic

208 pigments are found exclusively in one algal class (e.g. alloxanthin which is only found in cryptophytes)

209 while others are the principal pigments of one class but are also found in other classes (e.g. fucoxanthin in

210 diatoms and some haptophytes). The presence or absence of these diagnostic pigments can provide a

211 simple guide to the composition of a phytoplankton community including identifying classes of small

212 flagellates that cannot be determined by light microscopy techniques. In this study the presence of

213 fucoxanthin has been used to indicate diatoms; peridinin - dinoflagellates; 19' - hexanoyloxyfucoxanthin

214 (19HF) haptophytes; alloxanthin - cryptophytes; prasinoxanthin - prasinophytes; lutein - chlorophytes;

215 zeaxanthin - cyanobacteria and 19'-butanoyloxyfucoxanthin – pelagophytes (Vidussi *et al.*, 2001).

216

217 *2.4 Laboratory incubations*

218 During the voyage, a total of 58 phytoplankton primary production versus irradiance experiments were

219 conducted at discreet water depths for 15 locations across the continental shelf including King Sound (Fig.

220 1). The results from these experiments were used to characterise changes in phytoplankton photo-

221 physiology reported here and calculate depth-integrated primary production rates reported by McLaughlin

222 *et al.* (2019).

223

224 A small volume (7 mL) ^{14}Carbon (^{14}C) uptake method was used with a photosynthetron incubator (Lewis &

225 Smith 1983; Mackey *et al.*, 1995, 1997). Water samples collected during night-time casts were stored at

226 cool temperature in the dark until processing and incubation on the following day. A working solution for

227 each depth was created by inoculating sample water with ^{14}C (as NaH^{14}CO$_3$) to a final concentration of 1.0

228 µCi per 1.0mL seawater. Duplicate aliquots from each sampling depth were incubated for approximately 1 h

229 at seven main light levels, ranging from 0 to 750 µEm^{-2} s^{-1}, by using combinations of spectrally resolving

230 blue filters (LEE Filters # 119, 201, 202, and 203; for detailed wavelength specifications see

231 http://www.leefilters.com/lighting/colour-list.html). Duplicates were exposed to slightly different irradiance

232 levels by variability in the light output through distance between the light tubes with actual irradiance levels

233 (measured using a Biospherical Instruments Inc. 2100 PAR logger) used in the analyses to account for

234 inherent variability in the light output between the light tubes. Two 100 µL aliquots from each depth were

235 analysed to determine the total initial activity, as were duplicate 7mL time zeros (Mackey *et al.*, 1995).

236 Continuous surface seawater flow through the photosynthetron was used to regulate the temperature for all

237 incubations. Experiments were terminated through the addition of 0.25mL of 6M HCl and placing the

238 samples in an orbital shaker at ~180 revs min^{-1} for ca. 24 h to drive off any excess ^{14}C as CO$_2$ (Mackey *et*

239 *al.*, 1995). All samples were counted on-board the ship using an LKB Rackbeta liquid scintillation counter

240 the following day.

241

242 The model of Platt *et al.* (1980) was successfully fit to the majority of the photosynthesis-irradiance data

243 using the Matlab © function *nlinfit* according to

244 $$P = P_s\left(1 - e^{-\alpha I / P_s}\right)e^{-\beta I / P_s} \tag{1}$$

245   Where P is chlorophyll *a* specific photosynthesis in units of mg C mg Chl-a^{-1} hr^{-1}, P_S is the light saturated

246   photosynthetic rate in the absence of photo inhibition in units of hr^{-1}, α (photosynthetic efficiency) is the

247   initial slope of the productivity irradiance response in units of [mg C mg Chl-a^{-1} h^{-1} µEm^2 s], β is an index of

248   photo inhibition (same units as α), and I is irradiance in µEm^{-2} s^{-1}. The maximum photosynthetic rate, $P_{\max}$

249   is calculated as

250     $$P_{\max} = P_s \left[\alpha/(\alpha+\beta)\right]\left[\beta/(\alpha+\beta)\right]^{\beta/\alpha} \tag{2}$$

251   For the data collected within King Sound, the fitting of equation 1 failed due to scatter in the rate data

252   collected at high light intensities, and lack of any clear evidence of light inhibition, making estimation of the

253   model parameters uncertain. In these cases, a simplified model was easily fitted to the data by assuming β

254   equal to zero

255     $$P = P_s \left(1 - e^{-\alpha I/P_s}\right) \tag{3}$$

256   Where P_S is numerically equal to $P_{\max}$, and α retains its earlier meaning. Successful fitting of equation 3, in

257   cases where equation 1 had previously failed, reflected a general absence of any noticeable photo-

258   inhibition in the data.

259

260   **3. Results**

261   *3.1 Euphotic and mixed-layer depths*

262   Vertical profiles of σ_θ, and PAR show that, except at some of the KS and 50 m stations, the euphotic depth

263   is greater than the mixed-layer depth, and generally increases with distance offshore (Fig. 2). The lack of

264   any significant vertical gradient in water density or chl-*a* concentration suggests that all KS stations were

265   vertically well-mixed at the time of sampling (Fig. 3). This finding is consistent with the mixed-layer

266   extending to the seabed at all KS stations. The gradient of the natural logarithm of PAR versus depth

267   suggested differences in water clarity on different phases of the MS$_f$ tidal cycle, with steeper slopes on the

268   spring tide indicating light attenuation was higher (Fig. 3). *In-situ* light attenuation also tended to be stronger

269   at the deeper KS stations 24 and 84 than the shallower stations 25 and 85 located further upstream. The

270 combination of deeper water and stronger light attenuation resulted in the euphotic depth at the deeper KS

271 stations 24 and 84 being 18 and 14 m shallower than the seabed respectively, while the shallower KS

272 stations 25 and 85 further upstream had euphotic layers that extended over most of the water-column.

273 Calculations of mean and median PAR at the KS stations emphasize these differences with the mean

274 water-column PAR intensity approximately 1.5 times greater, and the median PAR intensity 4 or 5 times

275 greater at the shallower upstream sites (Table 1).

276

277 *3.2 Tidal mixing on the continental shelf*

278 On the continental shelf in the Kimberley Region tidal mixing plays a significant role in breaking down

279 stratification for depths shallower than 50 m. In Northern Australia, persistent cold patches have been found

280 to coincide with regions with significant variability in SST over the spring/neap cycle and coincide with

281 regions that have suppressed both seasonal and non-seasonal variance in SST (Wijffles *et al.*, 2018).

282 Studies of SST fronts in regions where tidal mixing is significant suggest that tidal mixing dominates for

283 $h/u^3 < 50$ with SST fronts observed for $65 < h/u^3 < 100$. On the Kimberley shelf region gradients in

284 SST climatology larger than 1° C per degree of latitude occur along the 50 m contour and correspond with

285 the region $65 < h/u^3 < 100$ calculated from the ROMS numerical model (Fig. 4). During spring tides, the

286 temperature front in the proximity of the 50 m contour corresponds to a numerically modelled mixing

287 timescale (T_M) of 24 hours (taking l as the water depth). For areas shallower than the 50 m depth, $T_M < 24$

288 hours during spring tides. For shelf regions where the depth is greater than 50 m, surface mixing (due to

289 the wind) become the dominant process driving mixing within the euphotic zone.

290

291 *3.3 Phytoplankton community composition*

292 Within King Sound (CTD stations 24–25, 84–85), the phytoplankton community was dominated by diatoms

293 as indicated by the relatively high concentrations of fucoxanthin (~30 to 55% of mean relative pigment

294 contribution). On the adjacent shelf, the community was increasingly dominated by cyanobacteria and

295 haptophytes with distance offshore, according to the relative increase in zeaxanthin and

296 hexanoyloxyfucoxanthin concentrations compared with other pigments (Fig. 5).

3.4 Phytoplankton light response curves

The photo-physiological (PI) response on the mid- and outer-shelf (Fig. 6; Table 2), where phytoplankton mainly grow in a sub-surface layer (McLaughlin *et al.*, 2019), is typical of observations made elsewhere in the open-ocean where the lack of available nutrients at the surface tends to limit phytoplankton growth to the base of the euphotic layer (Hanson *et al.*, 2007). Under these conditions the phytoplankton in the study region displayed relatively high photosynthetic efficiency with a median value of 0.121 mg C mg chl-*a*$^{-1}$ h^{-1} μEm^2 s (0.064 ≤ α ≤ 0.239), and relatively strong light inhibition with a median value of 0.017 mg C mg chl-*a*$^{-1}$ h^{-1} μE m^2 s (0.005 ≤ β ≤ 0.047), typical of low light adapted phytoplankton (Demers *et al.*, 1986). The PI response at depths less than the estimated mixed layer tended to be similar (Table 2; Fig. 6), whereas below the mixed layer vertical variation in the PI response was more noticeable with maximum photosynthetic rates reducing, and the onset of photo-inhibition occurring at lower light intensities, with increasing water-depth (Table 2; Fig. 6). Maximum photosynthetic rates on the mid- and outer-shelf ranged from 1.410 to 9.564, with a median value of 5.177 mg C mg chl-*a*$^{-1}$ h^{-1} (Table 2).

In contrast, the phytoplankton PI response in KS displayed a reduced median photosynthetic efficiency of 0.075 mg C mg chl-*a*$^{-1}$ h^{-1} μEm^2 s (0.056 ≤ α ≤ 0.175), an elevated median maximum photosynthetic rate of 8.889 mg C mg chl-*a*$^{-1}$ h^{-1} (4.554 ≤ P_{max} ≤ 14.589), and lack of any pronounced photo-inhibition compared with the shelf, (Fig. 7; Table 2), typical of light-acclimated phytoplankton (Demers *et al.*, 1986). The highest maximum photosynthetic rate was observed in KS under spring tide conditions at station 24 with values ranging from 9.320 to 14.589 mg C mg chl-*a*$^{-1}$ d^{-1} between the surface and 25 m water depth (Fig. 7). Similar results were obtained at the equivalent location during neap tide conditions (station 84) with values of P_{max} estimated to be between 9.704 and 13.689 mg C mg chl-*a*$^{-1}$ d^{-1} (Fig. 7). At stations 25 and 85, located in shallower water further upstream, values of P_{max} were significantly reduced with median values of 7.718 (7.341 ≤ P_{max} ≤ 8.458) and 4.762 (4.554 ≤ P_{max} ≤ 5.068) mg C mg chl-*a*$^{-1}$ d^{-1} respectively, and also displayed reduced vertical variability compared with stations 24 and 84 (Fig. 7; Table 2).

13

324 Results for the inner-shelf returned the lowest median values of both photosynthetic efficiency 0.048 (0.03

325 ≤ α ≤ 0.114) mg C mg chl-a^{-1} h^{-1} μEm^2 s , and maximum photosynthetic rate 3.8215 (3.021 ≤ P_{max} ≤

326 10.223) mg C mg chl-a^{-1} d^{-1} with weak rates of photo-inhibition 0.004 (0.000 ≤ β ≤ 0.004) mg C mg chl-a^{-1} h^{-}

327 ^{1} μEm^2 s compared with shelf positions further offshore and with stations inside KS (Figs. 6 & 7; Table 2).

328 Very little vertical variation in the PI response was observed on the inner shelf at stations 17 and 121,

329 where the mixed layer was estimated to extend to the seabed (Table 2; Fig. 6). In contrast, the relatively

330 shallow mixed-layers of 15 m and 18 m observed at stations 27 and 87 respectively corresponds with

331 observed vertical separation in the PI response at 0 and 10 m from the response at 25 and 50 m (Table 2;

332 Fig. 6).

333

334 *3.5 Relative importance of tidal mixing on phytoplankton photoadaptation*

335 Lewis *et al.* (1984) proposed a simple model to compare the (order of magnitude) importance of photo-

336 acclimation compared to vertical turbulent mixing based on a 1-D reaction-diffusion model. Assuming that

337 vertical variations with depth of phytoplankton photo-adaptive parameters are due to acclimation to the

338 local light climate, the dimensionless groups that control photo-acclimation are the irradiance aspect ratio

339 $k_d l$ and the relative mixing timescale $K_z \gamma / l^2$ where γ is the acclimation timescale of the photo-adaptive

340 parameter under consideration. The modulation of the M_2 tide across the spring neap cycle results in

341 variations in both vertical mixing and light attenuation due to enhanced bed shear stress and resuspension

342 of seabed sediment. Figure 8 presents the variation in photo-acclimation regime derived from MODIS

343 estimates of $k_d = k_{490}$ (IMOS, 2020) and vertical mixing from the ROMS model. For KS stations l is taken

344 as the local water depth and for all other stations l is taken to be nominally 40 m (Fig. 8). In KS vertical

345 turbulent mixing is dominant for photo-acclimation timescales greater than approximately 4 hours (Fig. 8a)

346 across the spring neap cycle. Timescales of vertical mixing in KS are consistent across the two stations

347 (Table 1), despite their differing depth due to vertical mixing scaling with the water depth in shallow open

348 channel flow (Fischer, 1963). However, spatial and temporal variations in light attenuation result in differing

349 light climates with station 24/84 having greater vertical variations in light (over a mixing timescale) than

350 station 25/85. At stations on the 50 m depth contour, photo-acclimation dominates vertical mixing for

351 adaptation timescales shorter than approximately 24 hours across the spring neap cycle. Depending on the

14

352 location, mixing timescales can vary by an order of magnitude across the spring neap cycle, with station

353 121 exhibiting the largest variation across the MS_f cycle. At stations further offshore photo-acclimation

354 dominates vertical mixing and vertical variations in photo-adaptive parameters are expected.

355

356 **4. Discussion**

357 King Sound has been identified as a pelagic productivity 'hotspot', despite reduced water clarity and low

358 ambient nutrient concentration compared with the adjacent shelf (McLaughlin *et al.*, 2019). Closer

359 investigation of the photo-physiological (PI) response of phytoplankton sampled in the region reported here,

360 suggests that photo-acclimation to periodic vertical tidal mixing, is responsible for the high rates of depth-

361 integrated productivity measured near the mouth of King Sound. Dissolved nutrient content was low and

362 constant with depth at the time of sampling the KS stations (McLaughlin *et al.*, 2019). We suspect that this

363 is due to the vertical tidal mixing which delivers a continuous supply of nutrients to the surface waters in

364 King Sound where they are taken up rapidly to support the rapid fixation of carbon (Berman-Frank &

365 Dubinsky, 1999).

366

367 Depending on topography and tidal amplitude, dissipation of semi-diurnal (M_2) tidal energy can result in

368 either continuous intense turbulent vertical mixing, or alternating periods of weak and relatively strong

369 mixing at M_2 frequency. Phytoplankton have developed an array of interrelated cellular mechanisms

370 allowing them to optimize light harvesting and utilization during exposure to changes in irradiance in a

371 temporally and spatially dynamic light field (Dubinsky & Stambler, 2009). These responses form the

372 phenotypic process termed photo-acclimation, which includes adjustment of optical properties involved in

373 the 'light reactions' of photosynthesis. The outcome of the photo-acclimation process mitigates extreme

374 light intensity fluctuations, reducing their effect to levels allowing growth beyond simple survival (Dubinsky

375 & Stambler, 2009). In an environment exposed to continuous intense mixing, the light conditions

376 experienced by phytoplankton can change faster than the physiological adjustment time of the cells, so that

377 phytoplankton can only adjust to the average light conditions (Demers & Legendre, 1982). In contrast,

378 phytoplankton exposed to alternating periods of weak and strong vertical mixing at M_2 frequency can

379 respond by changing their maximum photosynthetic rates (Fréchette & Legendre, 1982), depending on

380 their relative position in the water column compared to the vertical light gradient. Enhanced photosynthetic

15

381 activity has been observed for phytoplankton exposed to cyclical changes in light intensity, likely due to

382 reduced exposure of cells to bright light allowing high rates of photosynthesis to be maintained before

383 photo-inhibition occurs (Demers *et al.,* 1986). The MS_f tide modulates the amplitude of the M_2 tide changing

384 the vertical mixing conditions for phytoplankton; spring tides will favour more continuous mixing with shorter

385 periods of stability and stronger mixing, while neap tides will offer longer periods of stability and reduced

386 mixing rates.

387

388 The highest rates of photosynthesis were recorded for phytoplankton sampled near the mouth of KS (Fig.

389 1; stations 24 and 84), with little difference between spring and neap tide conditions (Fig. 7). Low

390 photosynthetic efficiency and absence of photo-inhibition at this location is characteristic of light-adapted

391 phytoplankton. Characteristic mixing timescales in KS were consistent across the two stations and are

392 significantly shorter than the M2 tide, suggesting that phytoplankton at these locations are exposed to

393 highly variable light conditions. Cyclical variations in the phytoplankton light climate at this location are

394 exaggerated by the fact that the photic layer covers little more than half of the total water column, meaning

395 that during a mixing cycle (where mixing extends all the way to the seabed) the phytoplankton will spend

396 some time in the 'dark'. Further upstream in King Sound (Fig. 1; stations 25 and 85) the mixing timescales

397 are the same, but the increased depth-averaged PAR at these locations (Table 1) as a result of the

398 similarity between mixing and photic depths, means that the phytoplankton experience reduced vertical

399 variations in light over a mixing timescale than they do at the deeper KS sites 24/84. This is reflected in the

400 vertical separation of the two main KS locations when plotted on Figure 8. We suspect therefore that a

401 more constant light climate is the main reason for the lower maximum photosynthetic rates measured at the

402 upstream KS sites, assuming that cyclical changes in light lead to higher maximum photosynthetic rates as

403 argued above. However, without information about nutrient uptake rates, nutrient limitation at the upstream

404 sites cannot be eliminated as a possible cause for the reduced photosynthetic rates. We note that,

405 sampling in KS generally took place close to high tide to aid ship navigation, and therefore may have

406 coincided with lower tidal velocities and lower rates of vertical mixing than experienced at other times of the

407 M_2 tidal cycle.

408

16

409 Photo-acclimation and photo-adaptation in many cases have been used as synonyms; however, more

410 recently, acclimation is reserved for phenotypic changes taking place in response to environmental cues

411 during the lifetime of the cell, while adaptation is usually used for genomic changes occurring in a

412 population on an evolutionary time scale (Dubinsky & Stambler, 2012). Blau *et al.* (2012) observed that

413 short-term fluctuations of coastal phytoplankton were dominated by periodicities of 6 hours 12 min, 12

414 hours 25 min and 24 hours. They concluded that the tidal cycle is a major determinant of phytoplankton

415 fluctuations at several different time scales. The mixing time scale calculated during the spring tide in Kind

416 Sound was ~3.5 hours, less than the 6 hour 12 min, period of the semi-diurnal tides found by Blau *et al.*

417 (2012). From diagnostic pigments, we found the phytoplankton community in King Sound was dominated

418 by diatoms (Fig. 5), which has been shown in lab culture experiments to be adaptive to their environment

419 by changing their photosynthetic potential to meet the demands of the area (Lavaud *et al.*, 2007). Diatoms

420 also generally have higher nutrient demands than other phytoplankton species (Smetacek, 1985).

421 Consequently, frequently mixed environments with variable light conditions and high nutrient fluxes are

422 often dominated by diatoms (Demers *et al.*, 1986). In contrast, the offshore phytoplankton community was

423 dominated by smaller-celled haptophytes and cyanobacteria that have less ability to cope with a fluctuating

424 light climate as in some cases they have light specific genotypes (West & Scanlan, 1999).

425

426 Hanson *et al.* (2007) showed that small differences in light attenuation and photo-inhibition can cause a

427 shift from surface-dominated to deep chlorophyll maxima (DCM) - dominated populations, and significantly

428 affect computations of primary production. In offshore waters bathymetric separation of different taxa is

429 driven by photo-acclimation. Processes of photo-acclimation push the euphotic depth deeper where

430 photosynthetic gains surpass respiratory losses more so than would be possible without photo-acclimation

431 further down the water column (Dubinsky & Stambler, 2012). A recent assessment of the physical and

432 chemical oceanography indicated more stratified conditions offshore with a pool of nutrients observed at

433 ~70 m, and phytoplankton growth restricted to a sub-surface maximum (McLaughlin *et al.*, 2019), a similar

434 trend to that found by Hanson *et al.* (2007), and Lourey *et al.* (2012) in other areas along the Western

435 Australia coast. The observed PI response on the outer shelf (Fig. 6) is consistent with observations made

436 in similar stratified ocean conditions where phytoplankton adjust their photo-physiology for the shaded

437 conditions (Falkowski, 1984) encountered at the base of the euphotic layer. This is largely confirmed by the

17

438 relative position of the outer shelf stations in Figure 8 showing where a depth-dependant photo-acclimation

439 would be expected in water-column conditions at the offshore sites due to the reduced mixing.

440

441 Finally, it is interesting to note that maximum photosynthetic rates appear to be somewhat restricted in the

442 vicinity of the 50 m isobath (Fig. 6). Our analysis shows that this is a region of the shelf subject to strong

443 variations in the mixing time-scale (Fig. 8), and has confirmed earlier work (Cresswell & Badcock, 2000)

444 that it is associated with a tidal-mixing front distinguishing offshore stratified waters from well-mixed water

445 on the shoreward side (Fig. 4). The extent of vertical mixing in this case is related to tidal range and can be

446 much reduced on the neap tide (Cresswell & Badcock, 2000), which may explain the increased vertical

447 variation in PI response, compared with the spring tide (Fig. 6). Although the existence of tidal fronts is

448 known to affect phytoplankton physiology in various ways (Demers *et al.*, 1986), further investigation will be

449 needed to understand this particular case. The phytoplankton at the 50 m stations was composed of an

450 almost equal mix of diatoms typical of inshore waters, and smaller cells typical of the stations further

451 offshore.

452

453 **5 Conclusions**

454 PI incubations were obtained from 15 stations extending from within King Sound into coastal waters, across

455 the shelf towards offshore. This region of the shelf is subject to strong variations in water column stability

456 associated with a tidal-mixing front distinguishing offshore stratified waters from well-mixed water on the

457 shoreward side. Trends in the PI response and phytoplankton pigments demonstrate a partitioning of

458 phytoplankton taxa associated with water column conditions either side of this tidal-mixing front. Shelf and

459 offshore waters were characterised by smaller phytoplankton taxa eliciting a PI response consistent with

460 stratified ocean conditions. The phytoplankton here have adapted their photo-physiology for the darker

461 conditions encountered at the base of the euphotic layer, where a trade-off between light for photosynthesis

462 and access to the deeper pool of nutrients yields the greatest success. In King Sound the phytoplankton

463 community was comprised mostly of diatoms with the region identified as a pelagic productivity 'hotspot',

464 despite reduced water clarity and low ambient nutrient concentrations compared with the adjacent shelf.

465   Here phytoplankton PI response displays low photosynthetic efficiency and an absence of photo-inhibition

466   characteristic of light-adapted phytoplankton.

467

468   Remote sensing and numerical modelling suggest that spatial and temporal variations in tidal mixing drive

469   changes in light variability and in photo-acclimation. Investigation of the photo-physiological response of the

470   phytoplankton in King Sound, suggests that photo-acclimation to alternate weak and strong mixing exposes

471   them to cyclical changes in light intensity delaying the onset of photo-inhibition. This allows higher

472   maximum photosynthetic rates to be attained. Phytoplankton experience the largest variations in light over

473   short timescales in King Sound where diatoms thrive since they have the capacity to rapidly acclimate to

474   water column light conditions by adjusting pigment within the cell. This photo-acclimation strategy is

475   responsible for the high rates of depth-integrated productivity measured in the estuary.

476

477

19

References

Auclair, J. C., Demers, S., Frechette, M., Legendre, L. 1982. High frequency endogenous periodicities synthesis in estuarine phytoplankton. Limnology 348-352.

Anon, 1972. Australia Pilot. In: North, North- West, and West Coasts of Australia from the West Entrance of Endeavour Strait to Cape Leeuwin, sixth ed., vol. 5 (Hydrographer of the Navy).

Behrenfeld, M. J., O'Malley, R. T., Boss, E. S., Westberry, T. K., Graff, J. R., Halsey, K. H., Milligan, A.J., Siegel, D.A., Brown, M.B. 2015. Revaluating ocean warming impacts on global phytoplankton. Nature Climate Change 6: 323–330.

Berges JA, Charlebois DO, Mauzerall DC, Falkowski PG (1996) Differential effects of nitrogen limitation on photosynthetic efficiency of photosystems I and II in microalgae. Plant Physiology 110: 689–696.

Berman-Frank I, Dubinsky Z (1999) Balanced growth in aquatic plants: myth or reality? Phytoplankton use the imbalance between carbon assimilation and biomass production to their strategic advantage. Bioscience 49: 29–37

Blain, S., Renaut, S., Xing, X., Claustre, H., Guinet, C. 2013. Instrumented elephant seals reveal the seasonality in chlorophyll and light-mixing regime in the iron-fertilized Southern Ocean: chlorophyll and light in Southern Ocean. Geophysical Research Letters 40: 6368–6372.

Blauw, A. N., Benincà, E., Laane, R. W., Greenwood, N., Huisman, J. 2012. Dancing with the tides: Fluctuations of coastal phytoplankton orchestrated by different oscillatory modes of the tidal cycle. PLoS One. 7: e49319.

Calbet, A., Agersted, M. D., Kaartvedt, S., Møhl, M., Møller, E. F., Enghoff-Poulson, S., Paulsen, M. L., Solberg, I., Tang, K. W., Tönnesson, K., Raitos, D. E., Nielsen, T. G. (2015) Heterogenous distribution of plankton within the mixed layer and its implications for bloom formation in tropical seas. Scientific Reports. 5 (11240). doi.org/10.1038/srep11240.

Cardol P., Bailleul B., Rappaport F., Derelle E. (2008) An original adaptation of photosynthesis in the marine green alga Ostreococcus. Proc Natl Acad Sci USA 105: 7881–7886

Cherukuru, N., Dekker, A.G., Hardman-Mountford, N.J., Clementson, L.A., Thompson, P.A. 2019. Bio-optical variability in multiple water masses across a tropical shelf: Implications for ocean colour remote sensing models. Estuarine, Coastal and Shelf Science 219: 223-230.

Clementson, L.A., Parslow, J.S., Turnbull, A.R., Bonahm, P. 2004. Properties of light absorption in a highly coloured estuarine system in south-east Australia which is prone to blooms of the toxic dinoflagellate Gymnodinium catenatum. Estuarine, Coastal and Shelf Science 60: 101-112.

Cloern, J.E., 1991. Tidal stirring and phytoplankton bloom dynamics in an estuary. Journal of Marine Research 49: 203-221.

Cresswell, G.R., Badcock, K.A. 2000. Tidal mixing near the Kimberley coast of NW Australia. Marine and Freshwater Research 51: 641-646.

de Boyer Montégut, C., Madec, G., Fischer, A.S., Lazar, A., Iudicone, D. 2004. Mixed layer depth over the global ocean: An examination of profile data and a profile-based climatology. Journal of Geophysical Research 109 (C12): 1-20.

Demers, S., Legendre, L. 1982. Water column stability and photosynthetic capacity of estuarine phytoplankton: long-term relationships. Marine Ecological Progress Series 7: 337-340

Demers, S., Legendre, L., Therriault, J. C. 1986. Phytoplankton reponses to vertical tidal mixing. In: Bowman, M. J., Barber, R. T., Mooers, C. N. K. (Eds), Lecture Notes on Coastal and Estuarine Studies. Springer-Verlag Publishing, New York, pp. 1-40.

Domingues, R. B., Anselmo, T. P., Barbosa, A. B., Sommer, U., Galvão, H. M. 2010. Tidal variability of phytoplankton and environmental drivers in the freshwater reaches of the Guadiana estuary (SW Iberia). International Review of Hydrobiology 95: 352–369.

Dubinsky, Z., Stambler, N. 2009. Photoacclimation processes in phytoplankton: mechanisms, consequences, and applications. Aquatic Microbial Ecology 56: 163–176.

Falkowski, P.G. 1980. Light and shade adaptation in marine phytoplankton. In: Primary Productivity in the Sea, pp. 99-119. P.G. Falkowski (ed.). Plenum Press, New York.

Falkowski, P.G. 1984. Physiological responses of phytoplankton to natural light regimes. Journal of Plankton Research 6: 295-307.

Falkowski, P.G., Laroche, J. 1991. Acclimation to spectral irradiance in algae. Journal of Phycology 27: 8-14.

Feng, M., Slawinski, D., Shimizu, K., Zhang, N. 2017. Climate change: knowledge integration and future projection. Final Report of Project 2.2.7 prepared for the Kimberley Marine Research Program, Western Australian Marine Science Institution, Perth, Western Australia, 50 pp.

Fischer, H. B. 1973. Longitudinal Dispersion and Turbulent Mixing in Open-Channel Flow. Annual Review of Fluid Mechanics, vol. 5, no. 1, 59–78.

Fréchette, M., Legendre, L. 1982. Phytoplankton photosynthetic response to light in an internal tide dominated environment. Estuaries 5: 287-293.

Hanson, C. E., Pesant, S., Waite, A. M., Pattiaratchi, C. B. 2007. Assessing the magnitude and significance of deep chlorophyll maxima of the coastal eastern Indian Ocean. Deep-Sea Research II 54: 884-901.

Herzig, R., Falkowski, P.G. 1989. Nitrogen limitation in Isochrysis galbana (Haptophyceae). 1. Photosynthetic energy conversion and growth efficiencies. Journal of Phycology 25:462–471.

Holloway, P.E., Chatwin, P.G., Craig, P. 2001. Internal Tide Observations from the Australian North West Shelf in Summer 1995. Journal of Physical Oceanography 31(5): 1182-1199.

Hooker, S.B., Van Heukelem, L., Thomas, C.S., Claustre, H., Ras, J., Schlüter, L. Clementson, L., Linde, D., Eker-Develi, E., Berthon, J-F., Barlow, R., Sessions, H., Ismail, H., Perl, J. 2009. The CSIRO method, in The Third SeaWiFS HPLC Analysis. Round-Robin Experiment (SeaHARRE-3). NASA Tech. Memo. 2009-215849, NASA Goddard Space Flight Center, Greenbelt, Maryland, 97 pp.

Houliez, E., Lizon, F., Artigas, L.F., Lefebvre, S., Schmitt, F.G., 2013. Spatio-temporal variability of phytoplankton photosynthetic activity in a macrotidal ecosystem (the Strait of Dover, eastern English Channel). Estuarine, Coastal and Shelf Science 129: 37-48.

IMOS. 2020. MODIS ocean colour satellite record from 2002 – 2020, https://portal.aodn.org.au/search?uuid=97b9fe73-ee44-437f-b2ae-5b8613f81042, accessed 14-04-2020.

Jeffrey, S.W., Vesk, M., 1997. Introduction to marine phytoplankton and their pigment signatures. In: Jeffrey, S.W., Mantoura, R.F.C., Wright, S.W. (Eds.), Phytoplankton Pigments in Oceanography: Guidelines to Modern Methods. UNESCO Publishing, Paris, pp. 37-84.

Jouenne, F., Lefebvre, S., Véron, B., Lagadeuc, Y. 2005. Biological and physiochemical factors controlling short-term variability in phytoplankton primary production and photosynthetic parameters in a macrotidal ecosystem (eastern English Channel). Estuarine, Coastal and Shelf Science 65: 421–439.

22

586 Kirk, J.T.O., Tilney-Bassett, R.A.E. 1978. The Plastids. Their chemistry, structure, growth and inheritance.
587   Elsevier/North-Holland Biomedical Press, Amsterdam. 2nd edition. 960 pp.

588 Larkum, A.W., Vesk, M. 2003. Algal plastids: Their fine structure and properties. In Larkum, A.W., Douglas,
589   S.E. Raven, J.A. (eds), Photosynthesis in algae, Kluwer Academic Publ, Dordrecht, The
590   Netherlands, pp. 11-28.

591 Lavaud, J., Strzepek, R.F., Kroth, P.G. 2007. Photoprotection capacity differs among diatoms: Possible
592   consequences on the spatial distribution of diatoms related to fluctuations in the underwater light
593   climate. Limnology and Oceanography 52(3): 1188–1194.
594
595 Lewis, M.R., Smith, J.C., 1983. A small volume, short incubation-time method for measurement of
596   photosynthesis as a function of incident irradiance. Marine Ecology-Progress Series 13: 99–102.

597 Lewis, M.R., Cullen, J.J., Platt T. 1984. Relationships between vertical mixing and photoadaptation of
598   phytoplankton: similarity criteria. Marine Ecology Progress Series 15: 141-149.

599 Lewitus, A. J., Koepfler, E. T., Morris, J. T. 1998. Seasonal variation in the regulation of phytoplankton by
600   nitrogen and grazing in a salt-marsh estuary. Limnology and Oceanography 43: 636–646.

601 Lourey, M.J., Thompson, P.A., McLaughlin, M.J., Bonham, P., Feng, M., 2012. Primary production and
602   phytoplankton community structure during a winter shelf-scale phytoplankton bloom off Western
603   Australia. Marine Biology 160: 355‑369.

604 Lucas, L.V., Koseff, J.R., Monismith, S.G., Cloern, J.E., Thompson, J.K., 1999. Processes governing
605   phytoplankton blooms in estuaries. II: The role of horizontal transport. Marine Ecology Progress
606   Series 187: 17-30.

607 Mackey, D.J., Parslow, J., Higgins, H.W., Griffiths, F.B., O'Sullivan, J.E., 1995. Plankton productivity and
608   biomass in the western equatorial Pacific: biological and physical controls. Deep-Sea Research 42:
609   499–533.
610 Mackey, D.J., Parslow, J.S., Griffiths, F.B., Higgins, H.W., Tilbrook, B., 1997. Phytoplankton productivity
611   and the carbon cycle in the western Equatorial Pacific under El Nino and non-El Nino conditions.
612   Deep-Sea Research II 44: 1951–1978.

613 Marra, J., Lance, V.P., Vaillancourt, R.D., Hargreaves, B.R. 2014. Resolving the ocean's euphotic zone.
614   Deep Sea Research 83: 45-50.

615 McLaughlin MJ, Lourey MJ, Hanson CE, Cherukuru N, Thompson PA, Pattiaratchi C. 2019. Biophysical
616   oceanography of tidally-extreme waters of the southern Kimberley coast, Western Australia.
617   Continental Shelf Research 173: 1-12.

618 Morel, A. 1991. Light and marine photosynthesis: a spectral model with geochemical and climatological
619   implications. Progress in. Oceanography 26: 263–306.

620 Parsons, T.R., Maita, Y., Lalli, C.M., 1989. A Manual of Chemical and Biological Methods for Seawater
621   Analysis. Pergamon Press, Toronto.

622 Platt, T., Gallegos, C.L., Harrison, W.G., 1980. Photoinhibition of photosynthesis in natural assemblages of
623   marine phytoplankton. Journal of Marine Research 38: 687–701.

624 Sathyendranath, S., Watts, L., Devred, E., Platt, T., Caverhill, C., Maass, H., 2004. Discrimation of
625   diatoms from other phytoplankton using ocean-colour data. Marine Ecology Progress Series 272:
626   59-68.

627 Savidge, G. 1979. Photosynthetic characteristics of marine phytoplankton from contrasting physical
628   environments. Marine Biology 53: 1-12.

629 Simpson, J.H., Hunter, J.R. 1974. Fronts in the Irish Sea. Nature 250: 404-406.

630 Smetacek, V.S. 1985. Role of sinking in diatom life-history cycles: ecological, evolutionary and geological
631   significance. Marine Biology 84: 239-251.

632 Smith R.C., Mobley C.D. 2008. Underwater light. In: Björn L.O. (ed) Photobiology: the science of life and
633   light, 2nd edition. Springer, New York, p 131–138.

634 Trigueros, J.M., Orive, E., 2000. Tidally driven distribution of phytoplankton blooms in a shallow, macrotidal
635   estuary. Journal of Plankton Research 22: 969–986.

636 Vidussi, F., Claustre, H., Manca, B.B., Luchetta, L., Marty, J. 2001. Phytoplankton pigment distribution in
637   relation to upper thermocline circulation in the eastern Mediterranean Sea during winter. Journal of
638   Geophysical Research 106: 19,939-19,956.

639 Vincent, W.F. 1980. Mechanisms of rapid photosynthetic adaptation in natural phytoplankton communities.
640   II. Changes in photochemical capacity as measured by DCMU-induced chlorophyll fluorescence.
641   Journal of Phycology 16: 568-577.

642 West, N.J., Scanlan, D.J. 1999. Niche-partitioning of Prochlorococcus populations in a stratified water
643   column in the eastern North Atlantic Ocean? Applied and Environmental Microbiology 65: 2585-
644   2591

645

646 Wetz, M.S., K.C. Hayes, A. J. Lewitus, J. L. Wolny, White, D.L. 2006. Variability in phytoplankton pigment
647   biomass and taxonomic composition over tidal cycles in a salt marsh estuary. Marine Ecology
648   Progress Series 320: 109–120.

649 Wijffels, S.E., Beggs, H., Griffin, C., Middleton, J.F., Cahill, M., King, E., Jones, E., Feng, M., Benthuysen,
650   J.A., Steinberg, C.R., Sutton, P. 2018. A fine spatial-scale sea surface temperature atlas of the
651   Australian regional seas (SSTAARS): Seasonal variability and trends around Australasia and New
652   Zealand revisited. Journal of Marine Systems 187: 156-196.

653 Wolanski, E., Spagnol, S. 2003. Dynamics of the turbidity maximum in King Sound, tropical Western
654   Australia. Estuarine Coastal and Shelf Science 56: 877-890.
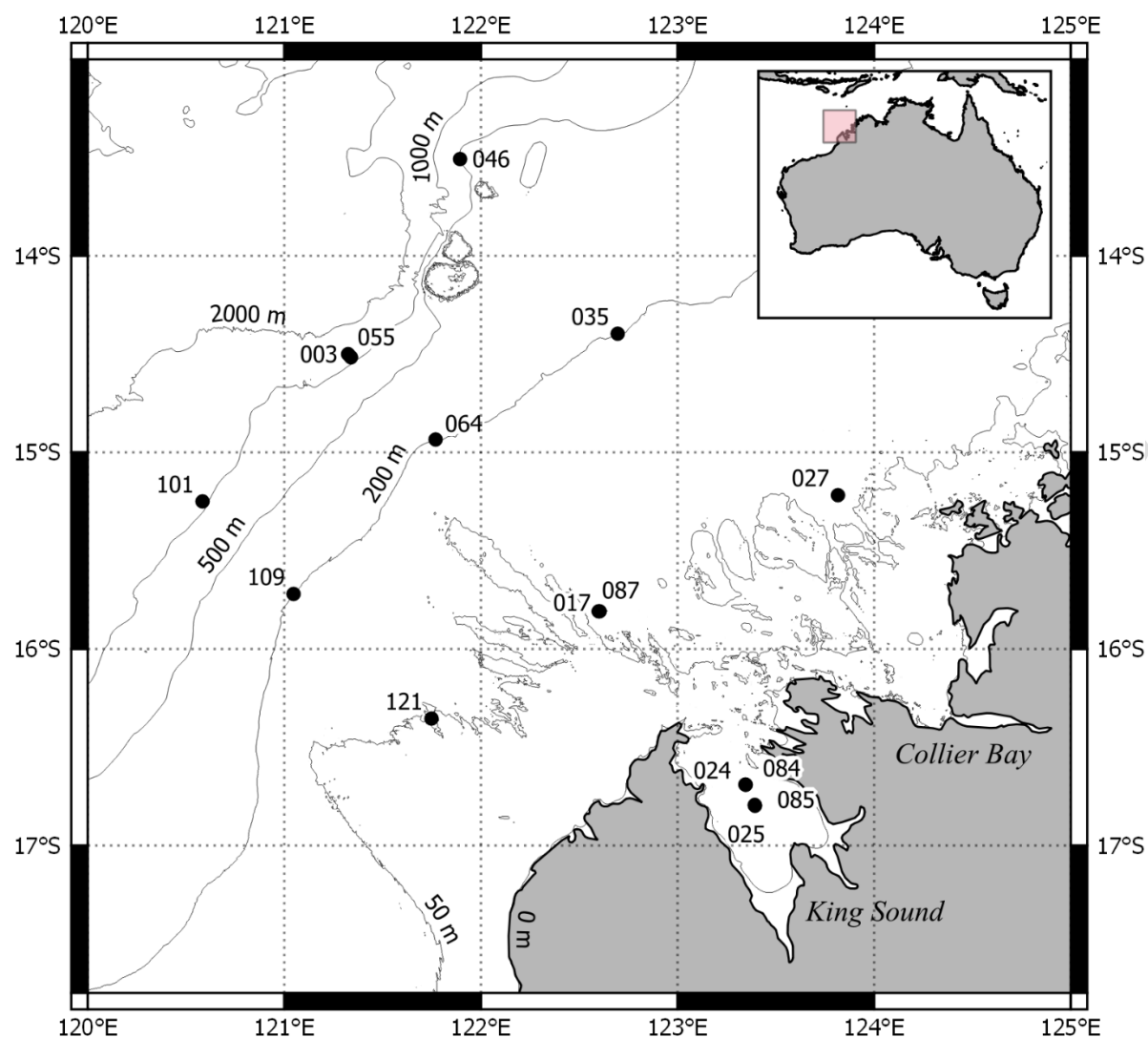
655

656
657
658
659

24

Figures and Tables

Fig 1. Location where phytoplankton productivity measurements, and supporting measurements of density, PAR, and chlorophyll fluorescence were made, within King Sound and on the adjacent shelf (solid circles).
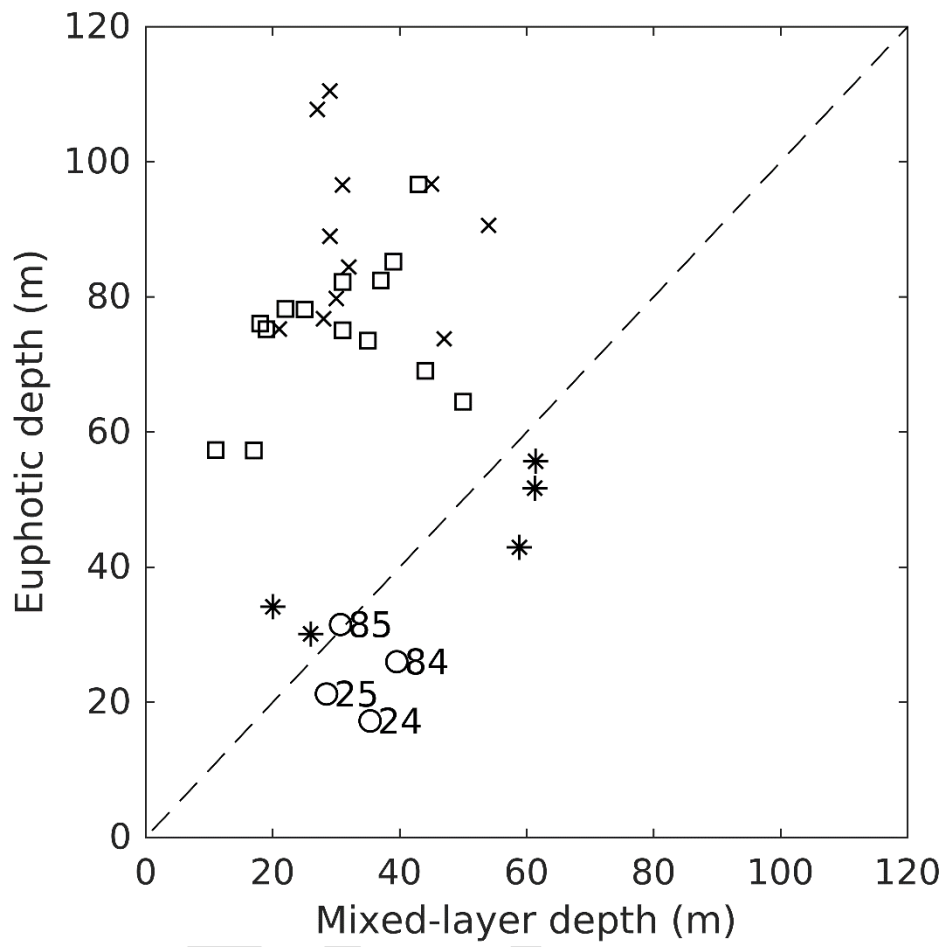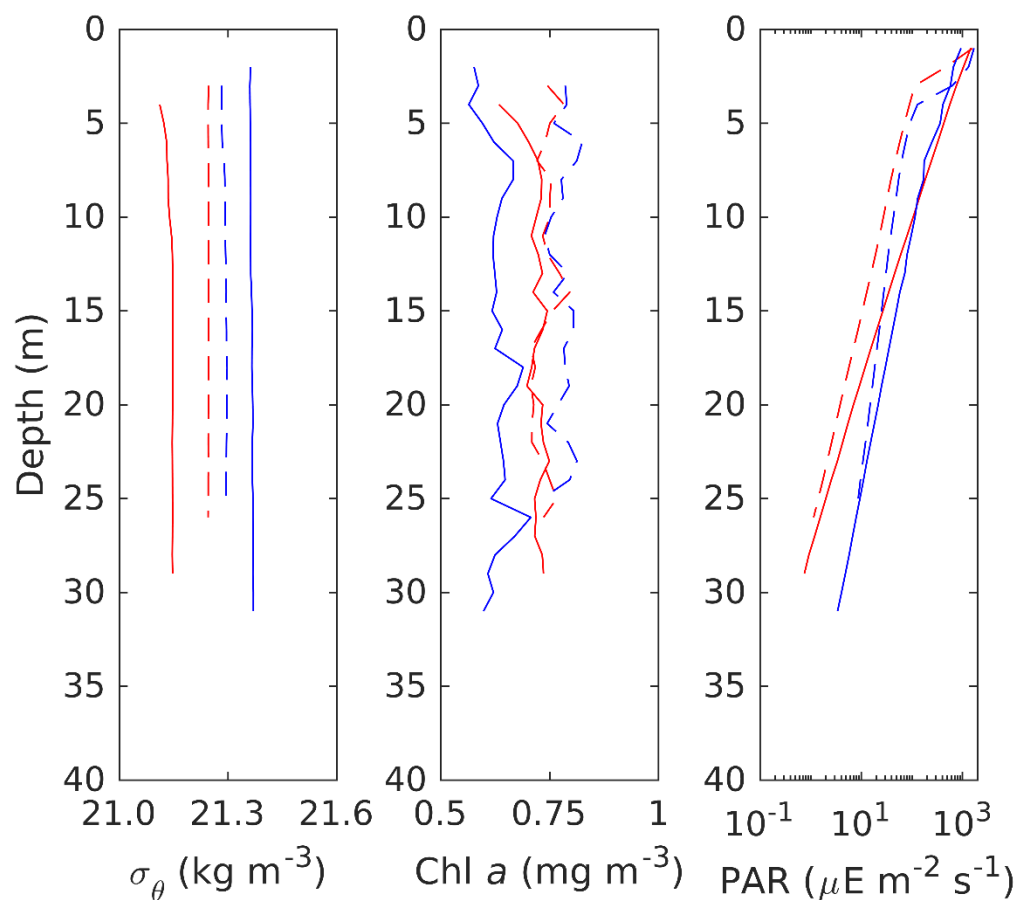
665

666   **Fig 2.** Variation of euphotic depth with mixed-layer depth at KS stations 24, 25, 84, and 85 (circles), and at
667   the 50 m (asterisks), 200 m (squares), and 1000 m (crosses) depth contours. The dashed line represents a
668   1:1 relationship between the two variables for reference.

669

671

672

Fig. 3. Vertical variation in potential density (σ_θ), chlorophyll *a* concentration (Chl *a*), and natural logarithm of photosynthetic radiation (PAR)   recorded at 1 meter vertical resolution during spring (solid lines) and neap (dashed lines) tide conditions for KS station 24 (red solid line), 25 (blue solid line), 84 (red dashed line) and 85 (blue dashed line).
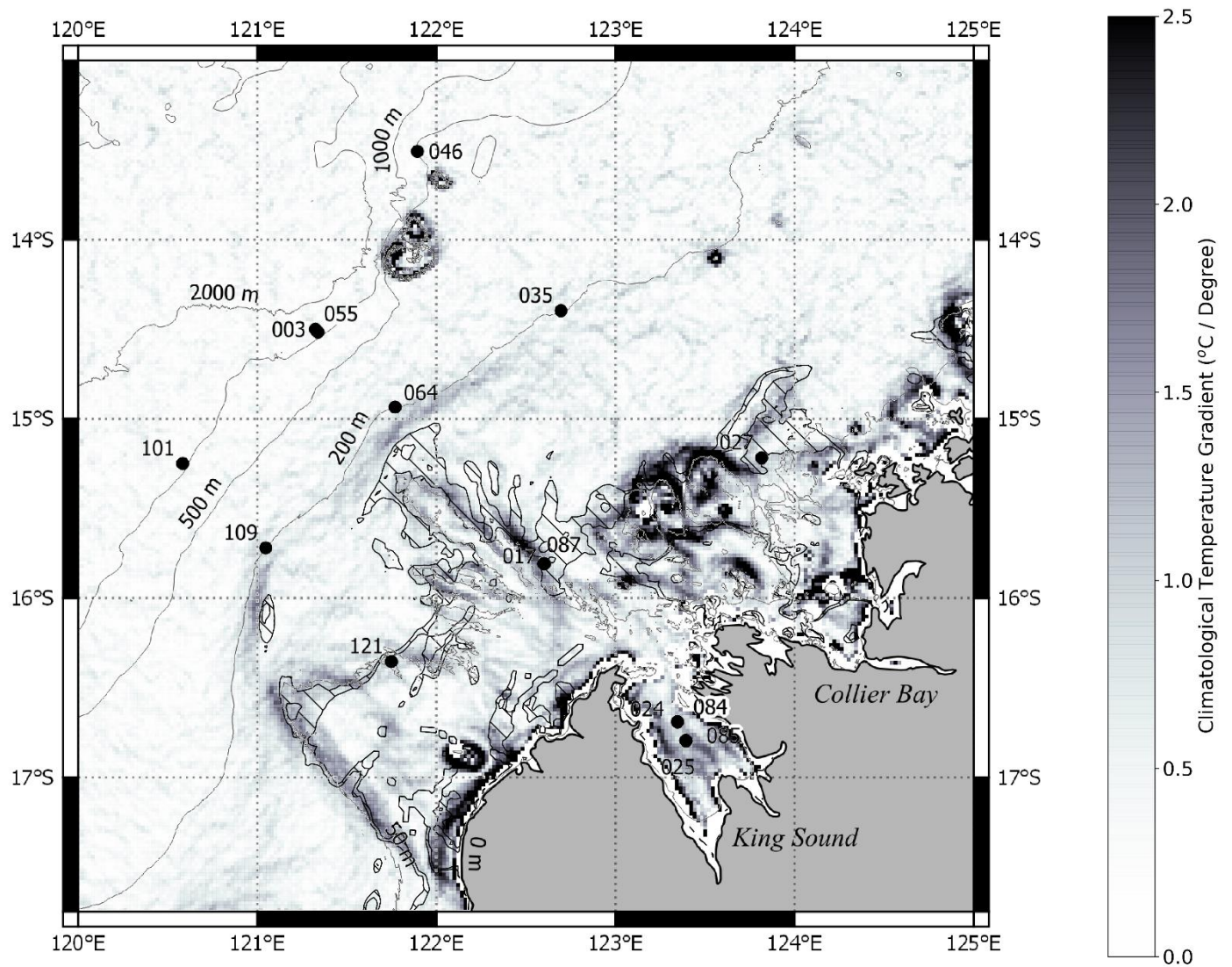
677

678

Fig. 4. Gradient in climatological temperature (shading) overlain with expected frontal region, $65 < h/U_0{}^3 <$ 100, (hatched contours) calculated from the ROMS hydrodynamic model.

681

682

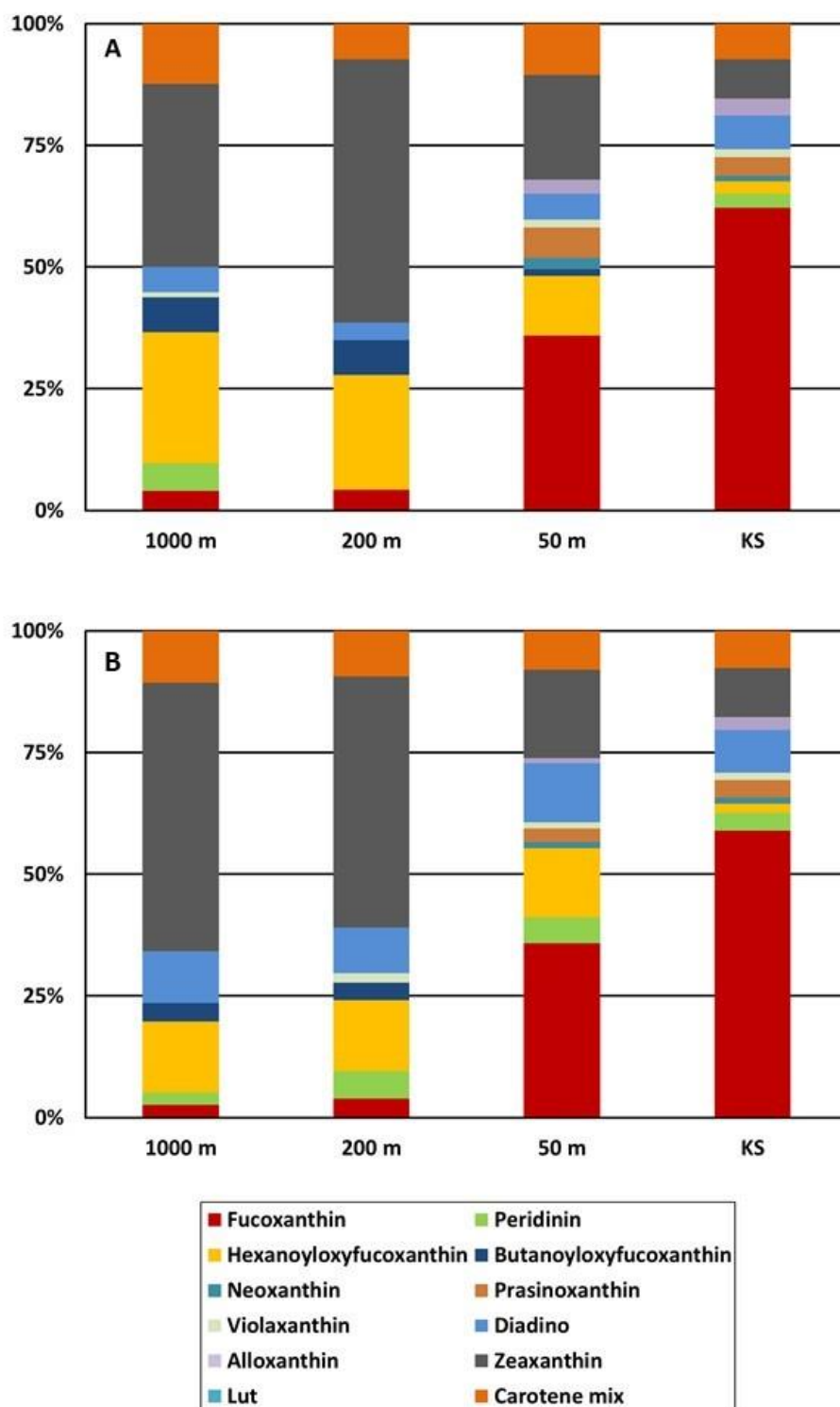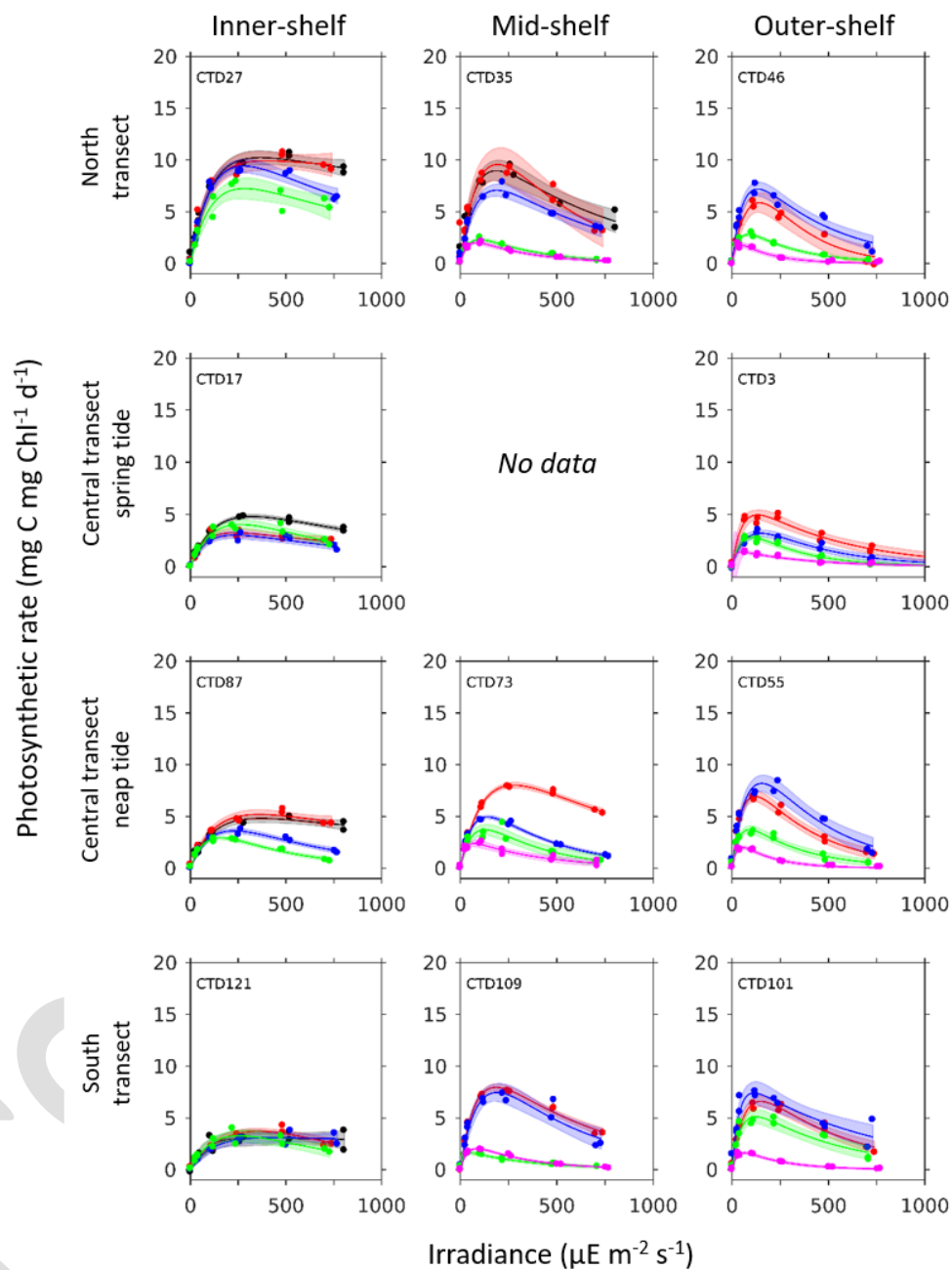683 **Fig 5.** Variation of phytoplankton pigment concentrations in King Sound (KS), and at the 50, 200 and 1000
684 m depth contours on the adjacent continental shelf during (a) spring, and (b) neap tidal conditions (adapted
685 from McLaughlin *et al.*, 2019).

Fig. 6. Variation of photosynthetic rate with irradiance for inner-, mid-, and outer-shelf locations along the northern, central and southern transects shown in Fig 1. The code in the upper right corner of each panel indicates the CTD station number and corresponds with station numbers shown in figure 1, and used in table 1. Note that the central transect was sampled twice, once during spring tide conditions, and again during neap tide conditions. No data is available for the mid-shelf location sampled on the central transect during spring tide. Lines are a non-linear fitting of equation 1 to the data points (filled circles), and shading shows the 95% confidence interval of the fitting. Colours represent different vertical water-column positions: black 0 m, red 10 m, blue 25 m, green 50 m and magenta 75 m. Fitting parameters are reported in Table 1.

688

689
690
691
692
693
694
695
696

697

698

Fig. 7. Variation in photosynthetic rate with irradiance measured during spring (left-hand panels) and neap (right-hand panels) tide conditions at two different locations (CTD 24/84, and CTD 25/85) within King Sound (See Fig 1 for locations). Lines are a non-linear fitting of equation 3 to the data points (filled circles), and shading shows the 95% confidence interval of the fitting. Colour represents different water-column depths: black 0 m, red 10 m, and blue 25 m. Fitting parameters are reported in Table 1.

704

Fig. 8. Variation in photoadaptation regime at the sampling locations for stages of the spring-neap cycle in the non-dimensional parameter space of irradiance aspect ratio $k_d l$ and mixing timescale ratio $K_z \gamma / l^2$ for (a) photoadaptation time scale $\gamma = 4$ hours and (b) $\gamma = 24$ hours. The dashed line ($K_z \gamma / l^2 = 1 - \exp(-k_d l)$) divides the parameter space into a region where photoadaptation dominates and a region where vertical mixing dominates (Lewis *et al.*, 1984).

32

Table 1. K_d, Mean and Median PAR values as indicators of the light climate within the mixed layer depth for both Spring and Neap tidal influenced production stations located within King Sound.

Station	MLD (m)	Mixing Time Scale (h)	K_d (m^{-1})	Mean PAR (mol photons $m^{-2}day^{-1}$)	Median PAR (mol photons $m^{-2}day^{-1}$)
24	36	3.6	0.27	48	4
25	29	3.5	0.22	74	20
84	40	6.6	0.18	66	13
85	31	6.6	0.15	101	48

714

Table 2. Fitted photosynthetic parameter value for each vertical water-column position sampled with shelf position.

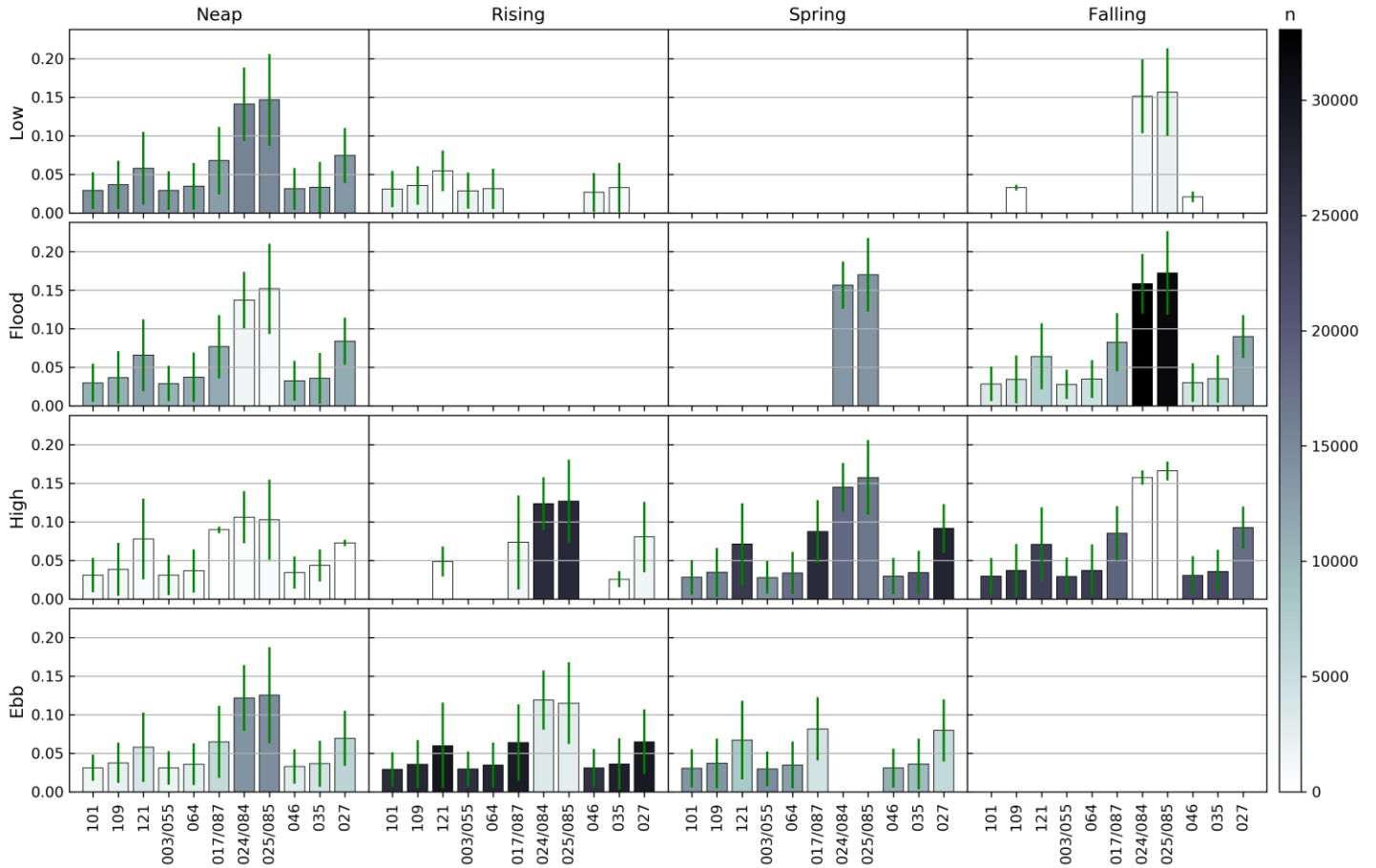| CTD	Shelf position (MS$_f$ tidal phase)	Seabed Depth (m)		MLD (m)	Parameter name	Fitted parameter value at each vertical water-column position sampled				
						0 m	*10 m*	*25 m*	*50 m*	*75 m*
24	King Sound *(spring)*	36		36	P_{max}	14.59	9.32	10.75		
					α	0.18	0.08	0.10		
					β	-	-	-		
25	King Sound *(spring)*	29		29	P_{max}	7.72	7.34	8.46		
					α	0.06	0.06	0.07		
					β	-	-	-		
84	King Sound *(neap)*	40		40	P_{max}	9.70	13.69	13.26	Not applicable	Not applicable
					α	0.09	0.07	0.09		
					β	-	-	-		
85	King Sound *(neap)*	31		31	P_{max}	4.77	5.07	4.55		
					α	0.06	0.08	0.07		
					β	-	-	-		
27	Inner shelf north transect	59		15	P_{max}	10.22	9.92	9.41	7.24	
					α	0.11	0.11	0.11	0.09	
					β	-	-	0.01	0.01	
17	Inner shelf central transect *(spring)*	62		62	P_{max}	4.81	3.24	3.02	4.04	
					α	0.05	0.05	0.04	0.05	
					β	0.01	-	-	0.01	
87	Inner shelf central transect *(neap)*	65		18	P_{max}	4.81	5.20	3.61	2.92	
					α	0.05	0.05	0.05	0.06	
					β	-	-	0.01	0.01	
121	Inner shelf south transect	62		61	P_{max}	3.07	3.23	3.09	3.27	
					α	0.04	0.04	0.03	0.04	
					β	-	-	-	0.01	
35	Mid shelf north transect	198		33	P_{max}	8.97	9.56	7.08	2.30	2.01
					α	0.16	0.15	0.12	0.07	0.08
					β	0.02	0.05	0.02	0.01	0.01
73	Mid shelf central transect *(neap)*	201		17	P_{max}	8.01	8.02	4.95	3.72	2.39
					α	0.09	0.09	0.11	0.09	0.12
					β	0.01	0.02	0.02	0.02	0.01
109	Mid shelf south transect	201		11	P_{max}	-	7.95	7.45	1.64	2.03
					α	-	0.14	0.12	0.13	0.08
					β	-	0.02	0.03	0.01	0.01
46	Outer shelf north transect	1007		45	P_{max}	-	5.87	7.19	2.80	1.80
					α	-	0.12	0.17	0.10	0.13
					β	-	0.10	0.03	0.02	0.01
3	Outer shelf central transect *(spring)*	1337		36	P_{max}	-	4.96	3.19	2.79	1.41
					α	-	0.12	0.06	0.08	0.11
					β	-	0.02	0.02	0.02	0.01
55	Outer shelf central transect *(neap)*	1049		52	P_{max}	-	6.93	8.19	3.72	2.00
					α	-	0.18	0.16	0.13	0.12
					β	-	0.03	0.04	0.02	0.02
101	Outer shelf south transect	1043		63	P_{max}	-	6.60	7.41	5.12	1.62
					α	-	0.14	0.24	0.14	0.08
					β	-	0.02	0.01	0.02	0.01

15

16

17

18

34

Fig. S1. Conditionally averaged MODIS k_d at 490 nm based on tidal phase of the semi-diurnal (high water, ebb tide, low water and flood tide) and spring-neap (spring, falling, neap and rising) cycles at the time of pixel acquisition. Cloud free pixels within 4 km of each station were utilised. Error bars show the 95% confidence interval of the mean and shading indicates the number of samples (n) within each class.

Evidence of phytoplankton light acclimation to periodic turbulent mixing along a tidally dominated tropical coastline.

M.J. McLaughlin[1,2]*, J. Greenwood[1], P. Branson[1,2], M.J. Lourey[3], C.E. Hanson[4]

[1]CSIRO Oceans and Atmosphere, Indian Ocean Marine Research Centre, M097, 64 Fairway, Crawley, Western Australia 6009
[2]University of Western Australia, Oceans Institute, Indian Ocean Marine Research Centre, M470 35 Stirling Highway, Crawley, Western Australia, 6009.
[3]BMT Global, 4/20 Parkland Rd, Osborne Park, Western Australia 6017, Australia
[4]Department of Education WA, 151 Royal Street, East Perth, Western Australia, 6004

Contents of this file

Introduction

Estimates of the light attenuation coefficient (k_d at 490 nm) were obtained from the MODIS ocean colour satellite record from 2002 – 2020, available through Australia's Integrated Marine Observing System (IMOS), for each in-situ sample location. At each station a harmonic fit of the water surface elevation from the Regional Ocean Modelling System (ROMS) model was calculated to provide a 20-year timeseries of predicted tide for each station. Observations of cloud-free pixels within 2 km of each station were classified according to the tidal phase of the semi-diurnal (high water, ebb tide, low water and flood tide) and spring-neap (spring, falling, neap and rising) cycles at the time of pixel acquisition. Within each tide phase class, the mean and standard deviation of k_d was calculated to provide an estimate of changes in irradiance length scale (k_d^{-1}) compared to the mixing length scale (l).
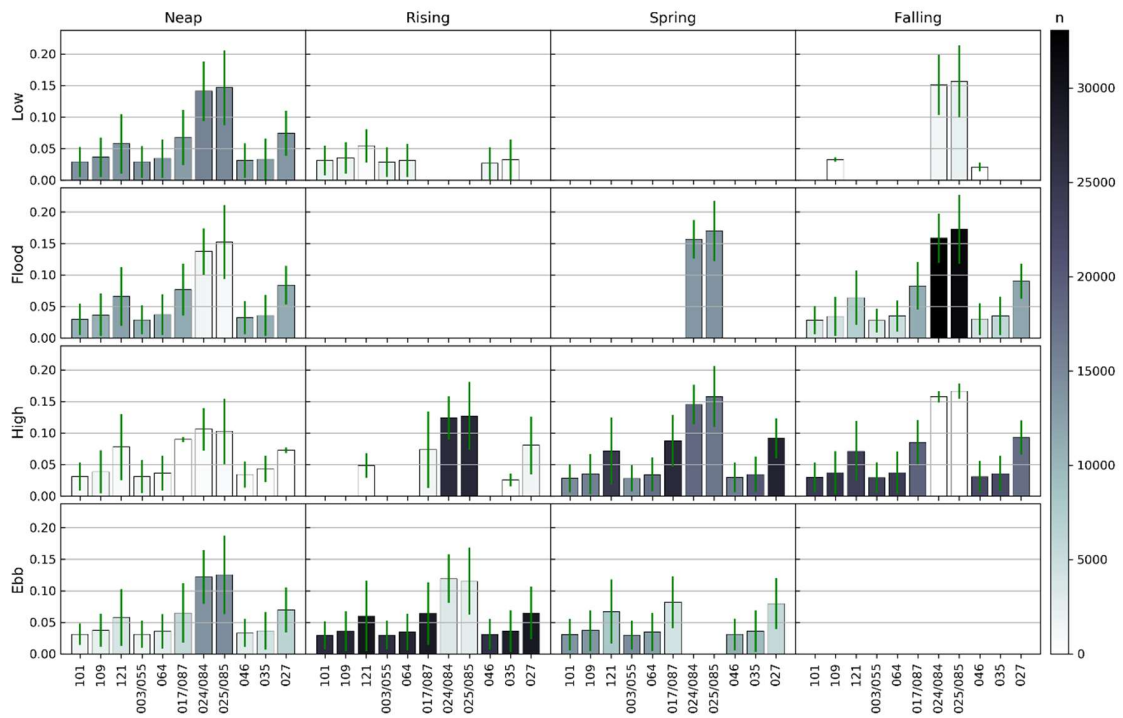

Figure S1. Conditionally averaged MODIS k_d at 490 nm based on tidal phase of the semi-diurnal (high water, ebb tide, low water and flood tide) and spring-neap (spring, falling, neap and rising) cycles at the time of pixel acquisition. Cloud free pixels within 4 km of each station were utilised. Error bars show the 95% confidence interval of the mean and shading indicates the number of samples (n) within each class.